ChemMedChem

Chemistry Europe
European Chemical Societies Publishing

Accepted Article

Title: Synthesis and biological evaluation of pyrazoline and pyrrolidine-2,5-dione hybrids as potential antitumor agents.

Authors: Kalpana Tilekar, Neha Upadhyay, Franz-Josef Meyer-Almes, Fulvio Loiodice, Anisimova Natalia Yu, Spirina Tatiana, Darina V Sokolova, Galina B Smirnova, Jun-yong Choe, Vadim S Pokrovsky, Antonio Lavecchia, and Ramaa C S

To be cited as: *ChemMedChem* 10.1002/cmdc.202000458

Link to VoR: https://doi.org/10.1002/cmdc.202000458

WILEY-VCH

WILEY-VCH

FULL PAPER

Synthesis and biological evaluation of pyrazoline and pyrrolidine-2,5-dione hybrids as potential antitumor agents.

Kalpana Tilekar[a],Neha Upadhyay[a], Franz-Josef Meyer-Almes[b], Fulvio Loiodice[c], Anisimova Natalia Yu[d]., Spirina Tatiana S[d]., Sokolova Darina V[d]., Smirnova Galina B.[d], Jun-yong Choe[e], Pokrovsky Vadim S.*[d,f], Antonio Lavecchia*[g] , C S Ramaa*[a]

[a] Title(s), Initial(s), Surname(s) of Author(s) including Corresponding Author(s)
[a] Kalpana Tilekar, Ms. Neha Upadhyay, Prof. C S Ramaa*
Department of Pharmaceutical Chemistry,
Bharati Vidyapeeth's College of Pharmacy,
Sector 8, CBD Belapur, Navi Mumbai, India.
E-mail: sinharamaa@yahoo.in

[b] Prof. Franz-Josef Meyer-Almes
Department of Chemical Engineering and Biotechnology,
University of Applied Science,
Darmstadt, Germany.

[c] Dr. Fulvio Loiodice
Department of Pharmacy-Drug Science,
University of Bari "Aldo Moro",
Via E. Orabona, 4, 70126 Bari, Italy

[d] Anisimova Natalia Yu., Spirina Tatiana S., Sokolova Darina V., Smirnova Galina B., Dr. Pokrovsky Vadim S*
Laboratory of combined therapy,
N.N. Blokhin Cancer Research Center,
Moscow, Russia.

[e] Dr. Jun-yong Choe
East Carolina Diabetes and Obesity Institute,
Department of Chemistry, East Carolina University,
Greenville, North Carolina, USA.

[f] Dr. Pokrovsky Vadim S*.
Department of biochemistry,
People's Friendship University,
Moscow, Russia.
E-mail: v.pokrovsky@ronc.ru

[g] Prof. Antonio Lavecchia*
Department of Pharmacy, "Drug Discovery" Laboratory,
University of Napoli "Federico II",
Via D. Montesano, 49, 80131 Napoli, Italy.
E-mail: antonio.lavecchia@unina.it

Supporting information for this article is given via a link at the end of the document.

Abstract: In search of novel and effective antitumor agents, pyrazoline-substituted pyrrolidine-2,5-dione hybrids were designed, synthesized and evaluated in silico, *in vitro* and *in vivo* for anticancer efficacy. All the compounds exhibited remarkable cytotoxic effects in MCF7 and HT29 cells. The excellent antiproliferative activity towards MCF-7 (IC_{50} = 0.78±0.01 µM), HT29 (IC_{50} = 0.92±0.15 µM) and K562 (IC_{50} = 47.25±1.24 µM) cell lines, prompted us to further investigate the antitumor effects of the best compound **S2**. In cell cycle analysis, **S2** was found to disrupt the growth phases with increased cell population in G1/G0 phase and decreased cell population in G2/M phase. The excellent *in vitro* effects were also supported by inhibition of anti-apoptotic protein Bcl-2. *In vivo* tumor regression studies of **S2** in HT29 xenograft nude mice, exhibited equivalent and promising tumor regression with maximum TGI, 66 % (i.p. route) and 60 % (oral route) at 50 mg/kg dose by both the routes, indicating oral bioavailability and anti-tumor efficacy. These findings advocate that hybridization of pyrazoline and pyrrolidine-2,5-dioes holds promise for the development of more potent and less toxic anticancer agents.

1. Introduction

Despite the advancement of cancer therapies, current cancer therapeutics suffers due to toxicity and drug resistance issues[1]–[3], specifying the need of continued search of newer anticancer agents. Scaffold hybridization approach is a commonly used but effective way in the era of modern medicinal chemistry. It has been reported several times, that combining two scaffolds together to form a hybrid molecule exhibits enhanced activity

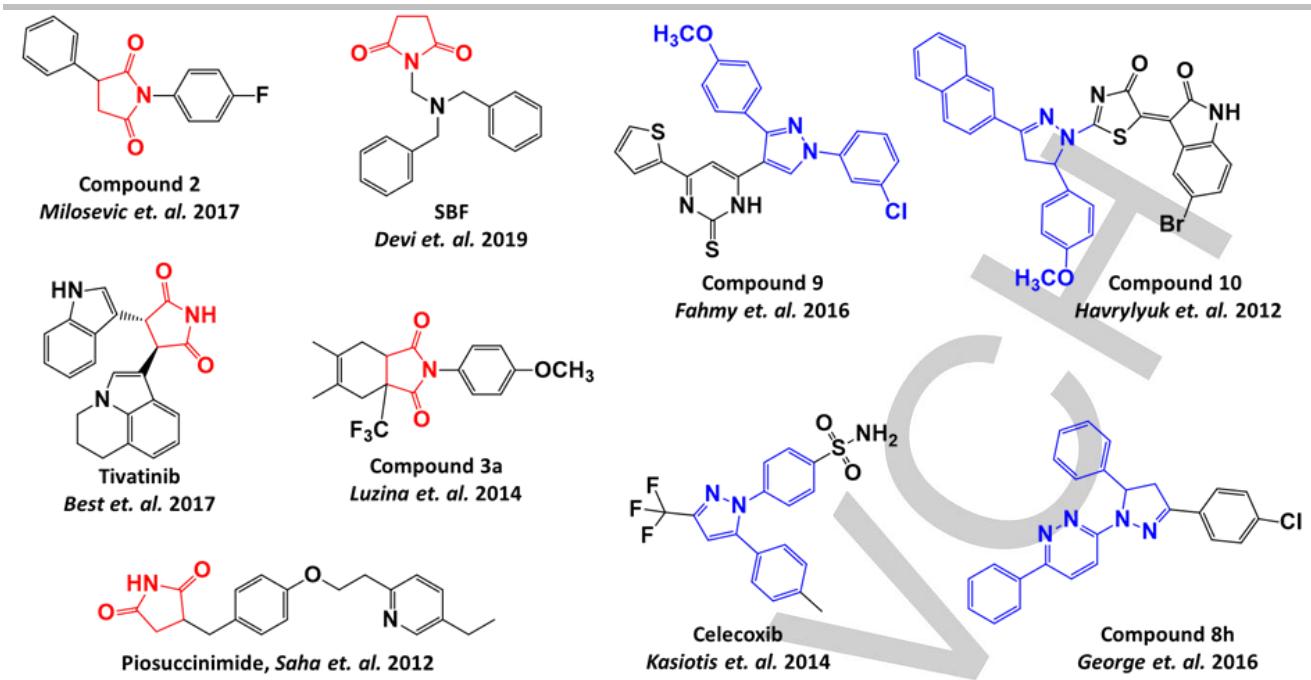

Figure 1. Potential anti-proliferative compounds with pyrrolidine-2,5-dione (red) and substituted pyrazoline (blue) moieties.

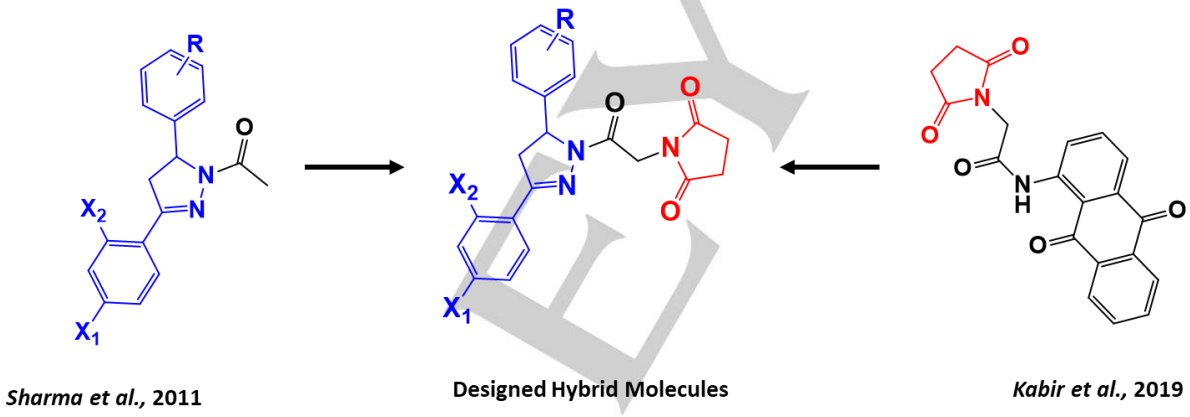

Figure 2. Designing of the hybrid molecules.

compared to agents with single scaffold[4]–[7]. In line with this approach, we designed and synthesised a hybrid series of novel molecules combining two pharmacologically attractive heterocycles, diaryl Pyrazoline and Pyrrodidine-2,5-dione.

Anti-cancer activity of pyrazolines reviewed by various authors revealed that N-substituted pyrazolines have exhibited antiproliferative and antitumor effects *in vivo* and *in vitro*[8][9] (**Fig. 1**). Recent literature showcases the potent cytotoxic activity of3,5-diaryl pyrazolines in different cancer cell lines[10][11]. They have been found to induce apoptosis, caspase activation, cause DNA intercalation, inhibit tubulin polymerization and autophagy in various cancer cells[12]–[17]. Moreover, these compounds have exerted anti-cancer effects through inhibition of various receptors/ enzymes/proteins involved in cancer cell division and growth[8]. Thus, it is evident that 3,5- diaryl pyrazolines can provide structural outlines for further anticancer drug development. Substituted 1,3-cyclopentadiones having structural framework (O=C-C(R)-C=O), which includes but not limited to 1,3-indanediones, thaizolidine-2,4-dione (TZD), phthalimides and pyrrolidine-2,5-diones (succinimides) have appealed to biologists and medicinal chemists since a long time. Pyrrolidine-2,5-dione is a privileged scaffold seen in bioactive compounds making it one of the most promising structural unit in drug discovery[18][19]. The antiproliferative effects of N-substituted pyrrolidine-2,5-diones have been reported against few cell lines such as hepatoma, lung, renal, breast cancer and leukaemia[20]–[25] (**Fig. 1**). Even though the primary antiproliferative activity has been explored to some extent, the overall antitumor mechanisms may be the most important and yet unexplored aspect.

Thus, hybrid molecules containing these two scaffolds were designed, synthesised, purified structurally characterised and evaluated for in vitro and *in vivo* antitumor activity.

2. Results and Discussion

2.1 Designing of the hybrid molecules

Earlier we had reported diaryl pyrazolines with remarkable anticancer activity against MCF-7 (Breast), HOP62 (lung), A498 (Renal) and MIAPACA2 (pancreatic)cell lines[26](**Fig. 2**). Thus, based on our past experience with this scaffold and literature evidences cited above, we selected diaryl pyrazoline as one portion of hybrid. In continuing efforts to discover novel antiproliferative agents, we have also reported TZD and its bio-isosteres with excellent activity against various leukemic and solid tumor cell lines[27]–[29]. In one such attempt we have reported anthraquinone based N-substituted pyrrolidine-2,5-diones as anticancer agents with cell line based antiproliferative effects in HL60 and K562 cell lines[30] (**Fig. 2**). For this reason, in current series we selected pyrrolidine-2,5-dione as other portion of the hybrid, since it is a bioisostere of TZD, it possesses antiproliferative potential and has not been much explored with respect to anticancer mechanism per se. In addition, the bio-isosteric replacement of TZD ring with pyrrolidine-2,5-dione has been reported to reduce toxicity and better the anticancer properties of thiazolidinediones[31].

Based on these observations, it was of interest to design hybrids incorporating 3,5-diaryl pyrazoline ring system onto nitrogen atom of pyrrolidine-2,5-dione (**Fig. 2**) in an attempt to obtain a novel anticancer agent.

2.2 Chemistry

Keeping in mind these designing considerations, we started with the synthesis of a series of compounds in which, we retained one or two fluorine atoms in a benzene ring and substituents with different electronic properties (halogen, methyl, methoxy) in the other one; in some cases, this last phenyl ring was replaced by a furan or a thiophene. The synthetic scheme to obtain the final derivatives **S1-S13** is outlined in **Scheme 1**. The procedure involves three steps: first step is the formation of chalcones, Schiff's bases **A1-A13**, by condensation of ketones such as acetophenone/4-fluoroacetophenone/2,4-difluoroacetophenone (1) and variously substituted aldehydes (2) under basic conditions. In second step, these chalcones are reacted with hydrazine hydrate in organic solvent to form the pyrazole ring; to this reaction mixture chloroacetyl chloride and potassium carbonate was added to obtain the formation of chloroacetyl derivatives of pyrazole **B1-B13**. The third step is an easy condensation of **B1-B13** with pyrrolidine-2,5-dione (succinimide, 3) in DMF, by catalysis with a mild base to give the final compounds **S1-S13**. All final compounds were structurally characterized by IR, ^{1}H-NMR, ^{13}C-NMR, and mass spectrometry; purity was higher than 95% and was established by HPLC.

FT-IR spectra of **S1-S13** displayed the characteristic absorption bands corresponding to stretching vibrations of pyrrolidine-2,5-dione in the region of 1699 to 1720 cm^{-1}, and tertiary in the region of 1666-1689 cm^{-1}. Proton NMR data of **S1-S13** displayed the four protons singlet of ethylene of pyrrolidine-2,5-dione in the region of 2.70-2.76 ppm. A singlet of 2 protons corresponding to methylene attached to carbonyl group was observed at 4.5-4.7 ppm. A multiplet or doublet of methylene of pyrazole ring was observed in the range of 3.8-3.9 ppm. ^{13}C-NMR exhibited signals for C=O carbon in the region of 160-180 ppm. Methylene carbons showed a peak at 40-50 ppm. Pyrrolidine-2,5-dione ethylene carbons found at around 27-28 ppm, methylene carbon of pyrazole ring were displayed at 40-45 ppm. Mass spectra in positive ionization scanning displayed the characteristic [M+H^{+}] peak at 100% m/z intensity for all the compounds.

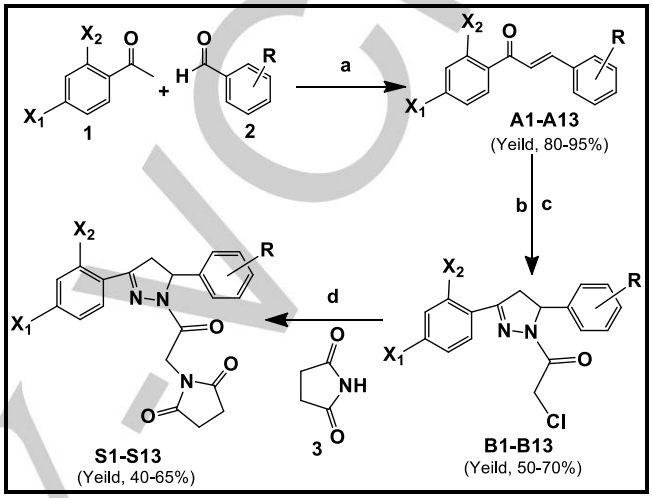

Scheme 1: Synthetic route followed to synthesize S1-S13. Reagents and conditions (a) Aqueous NaOH, EtOH, rt, 5-6 h; (b) $NH_2NH_2.H_2O$, $CHCl_3$, 80 °C, 12 h; (c) K_2CO_3, $ClCH_2COCl$, rt, 12 h; (d) K_2CO_3, DMF, rt, 6- 12 h.

2.3 In silico screening to determine physicochemical and pharmacokinetic profile of S1-S13 by using SwissADME platform

Apart from issues related to efficacy and toxicity, many times drug development failures are due to poor pharmacokinetic profile and bioavailability. Hence current trends of drug discovery have been observed making use of virtual *in vitro* testing methods and in silico property predictions to optimize lead compounds. swissADME is a freely accessible webtool to foresee pharmacokinetic and physicochemical properties of the new small molecules. This tool predicts the range of the physicochemical properties such as Molecular weight, solubility, partition coefficient, topological surface area etc., and pharmacokinetic properties such as absorption, distribution, metabolism, elimination of molecules, which are key parameters for lead molecule to progress to *in vivo* preclinical and clinical level[32]. In light of these predictions lead molecules can be modified or improvised such that it can exhibit all the desirable properties to be considered as lead-like or drug-like.

2D structures of the compounds, **S1-S13**, were sketched utilizing chemdraw ultra version 12.0 software, and were imported in the swissADME environment (http://www.swissadme.ch/) where SMILES of the structures were produced and used to run the swissADME tool. The readings for various physicochemical and pharmacokinetic parameters were generated, which were exported as CSV file and data was extracted. Bioavailability radar

Table 1. SwissADME predictions of physicochemical and pharmacokinetic properties for S1-S13.

Code	MW[a]	Fraction Csp3	RBs[b]	HBA[c]	HBD[d]	TPSA[e]	iLOGP[f]	ESOL Class[g]	GIA[h]	BBB[i] permeant	P-gp[j] substrate
S1	375.42	0.27	5	4	0	70.05	3.16	Soluble	High	Yes	No
S2	393.41	0.27	5	5	0	70.05	3.16	Soluble	High	Yes	No
S3	411.4	0.27	5	6	0	70.05	3.19	Soluble	High	Yes	No
S4	387.34	0.26	5	7	0	83.19	2.85	Soluble	High	No	No
S5	395.84	0.24	5	4	0	70.05	3.11	Soluble	High	Yes	No
S6	361.39	0.24	5	4	0	70.05	2.93	Soluble	High	No	No
S7	379.38	0.24	5	5	0	70.05	2.96	Soluble	High	Yes	No
S8	379.38	0.24	5	5	0	70.05	3	Soluble	High	Yes	No
S9	367.42	0.26	5	4	0	98.29	2.94	Soluble	High	No	No
S10	351.36	0.26	5	5	0	83.19	2.86	Soluble	High	No	No
S11	369.35	0.26	5	6	0	83.19	2.93	Soluble	High	No	No
S12	457.43	0.3	7	8	0	88.51	3.3	Soluble	High	No	No
S13	430.28	0.24	5	4	0	70.05	3.12	Moderately soluble	High	Yes	No

[a]-Molecular weight, [b]-Rotatable bonds, [c]- Hydrogen bond acceptors, [d]-Hydrogen bond donors, [e]- Topological surface area, [f]-octanol–water partition coefficient, [g]-Solubility class, [h]-Gastro-intestinal absorption, [i]-Blood brain barrier, [j]- P-glycoprotein

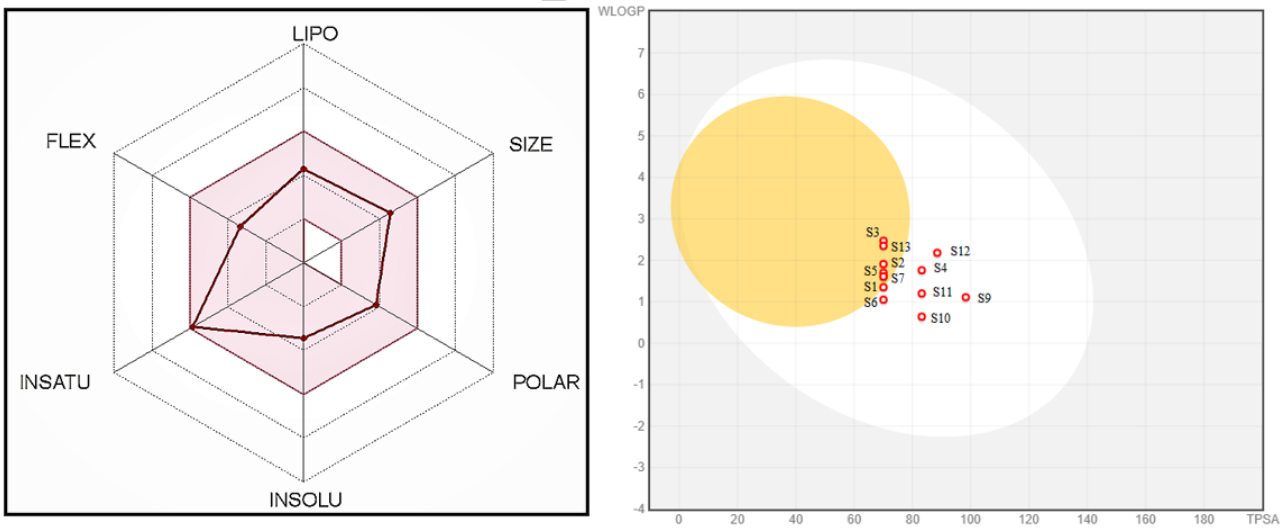

Figure 3. Left, Bioavailability radar plot of compound S2. Right, BOILED-Egg plot of S1-S13 generated in SwissADME environment

plots displayed by SwissADME tool were straight taken for the interpretation.

Data analysis revealed that, the molecular weights of the compounds **S1-S13** falls between 361.39 to 557.43 g/mol, ilogP values[33] were found in the range of 2.85 to 3.47, topological polar surface area, (TPSA) was ranging from 7.05 to 115.87 Å. The count of hydrogen bond acceptors, (HBA) were <10, and of hydrogen bond donors, (HBD) were <5. Out of 13 compounds, 12 compounds were predicted to be soluble and one was found to be moderately soluble. Gastrointestinal (GI) absorption for the all the compounds was predicted to be high. 55% of the compounds were found penetrating to BBA (blood–brain barrier). Also, compounds were predicted to non-substrates for P-glycoprotein,

Table 2. 50% Inhibitory concentration (IC_{50}) values of active S-series compounds in MCF7, HT29 and K562 cell lines obtained by MTT assay.

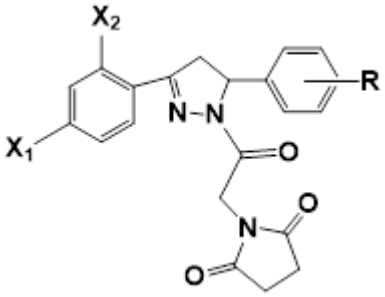

Code	X_1	X_2	R	MCF-7 (IC_{50} µM)	HT-29 (IC_{50} µM)	K562 (IC_{50} µM)
S1	H	H	4-CH_3	4.55±0.37	2.43±0.38	24.74±0.86
S2	F	H	4-CH_3	0.78±0.01	0.92±0.15	47.25±1.24
S3	F	F	4-CH_3	7.31±0.24	2.84±0.43	53.99±1.68
S4	F	F	2-Furyl in place of phenyl	8.62±0.07	1.99±0.34	40.85±1.84
S5	H	H	2-Cl	15.62±0.73	1.44±0.24	40.47±1.57
S6	H	H	H	0.42±0.13	3.99±0.44	40.4±1.30
S7	H	H	4-F	0.74±0.19	2.52±0.42	31.56±1.22
S8	F	H	H	8.90±0.36	3.91±0.38	46.06±1.21
S9	H	H	Thiophen-2-yl in place of phenyl	21.64±0.37	1.72±0.32	45.22±1.06
S10	H	H	2-Furyl in place of phenyl	4.12±0.60	1.66±0.45	39.42±1.91
S11	F	H	2-Furyl in place of phenyl	20.12±0.08	3.90±0.79	71.73±1.56
S12	F	F	3,4-Dimethoxy	2.02±0.12	2.57±0.39	48.75±0.01
S13	H	H	3,4-Dichloro	1.21±0.22	0.39±0.12	61.92±0.03
Pioglitazone	-	-	-	0.07±0.04	19.94±1.28	40.30±0.73
Paclitaxel	-	-	-	0.35±0.004	0.32±0.007	0.29±0.004

Experiments were performed in duplicates and values are presented as Mean±SD.

(P-gp). P-gp is found in various tissues and acts as efflux transporters, pushing the xenobiotics out from the cells, leading to enhanced clearance of these xenobiotics[34]. The bioavailability score was found to be 0.55 and compounds were predicted to drug-like, as indicted by Lipinski's rule of five[35], Muegge's filter[36], Veber's rule[37], Egan rule[38], and Ghose filter[39].

The Brain Or IntestinaL EstimateD permeation method (BOILED-Egg) is projected as a precise predictive model that give predictions for both brain and intestinal permeation and works by calculating the lipophilicity (WLOP) and polarity (TPSA) of small molecules. The BOILED-Egg model delivers a fast, reproducible, experimentally validated, intuitive, yet statistically robust method to forecast the passive GI absorption and brain penetration of small molecules, thus the BOILED-Egg can be of reliable support in the process of lead optimization[40]. Observation of the placement of our newly synthesized derivatives on BOILED-Egg plot (**Fig. 3**, **Right**), found that all the compounds were present either in yellow (yolk) or white zone, and none was deviating in grey area, indicating that will be highly passively absorbed in GI tract, thus can exhibit oral bioavailability. Out of 13 compounds, 7 compounds were found in yellow (yolk) zone, and are predicted to penetrant to Brain. This indicates both, chances of CNS adverse effects as well as possibility of usefulness to treat brain tumors. For this series of compounds, from *in vivo* efficacy studies (presented in section 2.8) it was observed that any of the treated animal did not exhibited any visible behavioral changes, which indicates that this series of compounds may not display any CNS

adverse effects, and also exhibited promising antitumor efficacy after oral administration.

The swissADME also generates a bioavailability radar plot for each compound, which gives likely contour of oral bioavailability of the compounds, the pink zone of the radar plot is the ideal zone indicating, place where the lead-like molecules are found. The six physicochemical properties measured to generate this ideal zone, are lipophilicity-LIPO, size-SIZE, solubility -INSOLU, polarity-POLAR, saturation-INSATU and flexibility-FLEX. Bioavailability radar plot of compounds, **S2** has been presented in **Fig. 3, Left**. The compounds **S1-S13** were observed to be situated in pink area of the radar plot. Thus, prediction data indicates that these series of compounds may display favorable pharmacokinetic and physicochemical profile to be drug-like molecules.

2.4 *In vitro* antiproliferative effects by MTT assay

The intriguing cytotoxic/antiproliferative effects in various tumor cells shown by both pyrrolidine-2,5-dione- and pyrazoline-based derivatives prompted us to investigate the activity of **S1-S13** in solid and hematological tumor cell lines. *In vitro* cytotoxicity of the compounds was determined by MTT assay utilizing three cell lines, myeloid leukemia cell line K562, breast cancer cell line MCF7, and colon cancer cell line HT29, as described previously[41][42]. Each cell line was exposed to test compounds for 48 hrs. Paclitaxel and Pioglitazone were used as standard references and untreated cells were used as negative control. Paclitaxel was selected as one of the standards as it is a clinically used anticancer agent, whereas Pioglitazone was chosen as second standard as it is a PPARγ agonist containing the TZD group bio-isostere of pyrrolidine-2,5-dione. The IC_{50} values are shown in Table 2 and mean cell viability plots are presented in Supplementary section, **Supplementary Fig.S3-S5**. All the compounds were found several times more active against MCF7 and HT29 as compared to K562. In MCF7 cell lines, compounds **S2, S6** and **S7** exhibited IC_{50} 0.78±0.01 µM, 0.42±0.13 µM and 0.74±0.19 µM, respectively. Against HT29, compounds **S2** and **S13** exhibited activity in sub-micromolar range with IC_{50} 0.92±0.15 µM and 0.39±0.12 µM, respectively. All remaining compounds exhibited IC_{50} values between 4 to 22 µM for MCF-7 cell lines and < 4 µM in HT29 cells. Almost all compounds exhibited moderate activity against K562 cell line in mid-micromolar range. When compared to standard Pioglitazone, most of the compounds exhibited much better antiproliferative effects towards HT29 and K562 cells. In addition, **S2** and **S13** displayed excellent antiproliferative effects in MCF7 and HT29 comparable to the clinical anticancer agent Paclitaxel. Thus, our newly synthesized pyrazoline-substituted pyrrolidine-2,5-dione series prove to be a promising series of compounds with outstanding antiproliferative profile in solid tumors.

2.5 Cell Cycle Analysis.

Compound **S2** was selected for further *in vitro* and *in vivo* study because of its cytotoxicity (IC_{50} = 0.92 µM) towards this tumor cell line that is about 20-fold higher than reference compound Pioglitazone and only 3-fold lower than Paclitaxel. The effect of treatment of **S2** on cell cycle distribution in K562 cells was performed on the basis of DNA content in K562 cells, after treatment with increasing concentrations of **S2** for 48 h by using Muse® Cell Cycle Kit (MCH100106 EMD Millipore Corp., USA). After 48 h exposure of K562 cells to **S2** at three increasing concentrations up to IC_{50} value, increase in number of cells in G0/G1 phase was observed in comparison with control cells (56% at IC_{50} concentration compared to 47% in control) (Supporting data, **Supplementary Table. ST3, Fig. S4)**. Also, decrease in the number of cells in the G2/M phase relative to the control cells was observed (21.5% at IC_{50} concentration compared to 30% in control).

2.6 Effect on Bcl-2 expression.

Bcl-2 alters the activity of a variety of cell signaling proteins involved in apoptosis, proliferation, and cell survival. Overexpression of Bcl-2 mediates resistance to apoptosis through alteration of other cell signaling pathways, such as cyclin D1/p27, p53/mdm2, and NF-κB[43], thus considered as anti-apoptotic protein. Hence, inactivation of this protein leads to unavailability of activated/phosphorylated form, offers a way to make tumor cells to undergo apoptosis. Effects of **S2** on expression levels of Bcl-2 protein were studied in K562 cells (**Fig. 4**). The cells were seeded in 96-well plates and incubated at 37 ºC in a 5% CO_2 atmosphere during 18 h, thereafter **S2** was added to the cells, and the incubation was continued for 48 or 72 h more (Supporting data, **Supplementary Table. ST4**). The experiments were performed as per the manufacturer's protocol using Muse® Bcl-2 Activation Dual Detection Kit (MCH200105 EMD Millipore Corp., USA). SPSS 21 software was used for statistical analysis. One-way ANOVA and post hoc Dunnett`s test was performed to assess differences between the individual groups against one control. Data are presented as mean±SD. P value <0.05 was considered statistically significant. Dose-dependent decrease was observed in the expression levels of phosphorylated Bcl-2 as compared to control cells (55.0% at IC_{50} concentration (p=0.008) or 64.0% at ½ IC_{50} concentration (p=0.034) compared to 85.0%in control). Thus, significant cytotoxic/antiproliferative effects can be attributed to inhibition of Bcl-2 protein.

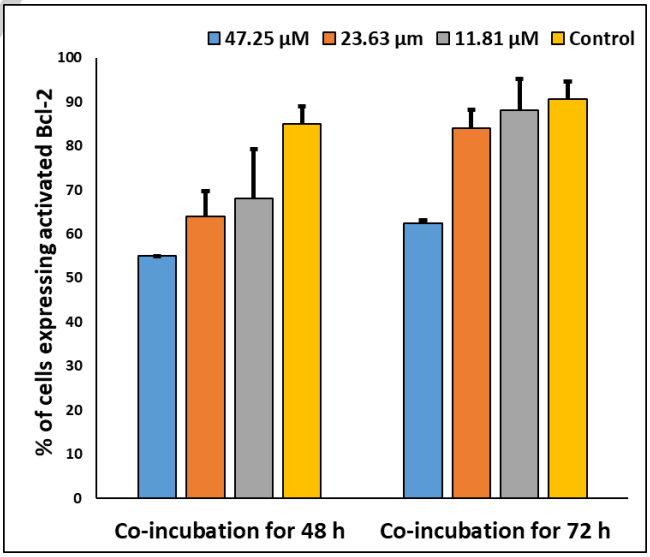

Figure 4. Graphical presentation of dose dependent decrease in expression of activated Bcl-2 after treatment with S2 for 48 h and 72 h in K562 cells. Values are presented as Mean of 3 experiments; error bars represent standard error of mean.

2.7 Docking at binding site of Bcl-2.

Bcl-2 is a pro-survival member of the Bcl-2 protein family characterized by a conserved hydrophobic groove on the surface. The α-helical BH3 domain of proapoptotic members of the Bcl-2 protein family (e.g. Bim, Bid, Puma, Bad) can bind to the hydrophobic groove of Bcl-2, thereby initiating the apoptosis cascade. It has been shown that small-molecule BH3 mimics, such as ABT-737 [44][45] or navitoclax [45][46], efficiently induce cell death in tumors. As dose dependent decrease was observed in levels of Bcl-2, we undertook docking analysis of **S2** at binding groove of Bcl-2. Docking was performed using Autodock Vina. At first, the docking procedure was validated by redocking the respective ligand into the crystal structure of complexes between Bcl-2 and two different small molecule ligands. Both redocked ligands showed excellent overlap with the corresponding crystallized ligand showing RMSD-values of 0.69 Å (PDB-ID 4AQ3) and 0.37 Å (PDB-ID 6GL8), respectively (Supporting data**, Supplementary Fig. S5**). Therefore, docking parameters were optimally suited for docking unknown compound **S2**. To rationalize the putative molecular interaction between of **S2** and Bcl-2, the two stereoisomers R-S2 and S-S2 with chiral carbon in the pyrazole ring were docked into two different crystal structures of Bcl-2 (PDB-IDs 4AQ3 and 6GL8). Differences in the crystal structures of Bcl-2 were attributed to a certain degree of flexibility around the binding groove and considered by an energy minimization of the original best docking pose within a radius of 10 Å around the ligand using MOE 2019 and AMBER14 force field. The prolonged ligand in the crystal structure PDB-ID 4AQ3 occupies most of the hydrophobic groove on the surface of Bcl-2, similar to the BH3-α-helix of proapoptotic proteins (**Fig. 5- A, B**). In contrast, the much smaller ligand from PDB-ID 6GL8 and R-S2 both occupy the deeper hydrophobic subpocket defined by F71, F63, M74, V92, L96 and do not cover the shallower distant second site (**Fig. 5- B, C, D**). R-S2 forms a hydrogen bond to R105 through a carbonyl oxygen next to the pyrazoline group (**Fig. 5-C, D**). In addition, R-S2 forms an intramolecular hydrogen bond, which fixes the ligand in a favorable pose, thereby reducing potential entropy losses. The aromatic groups of R-S2 show pi-stacking interactions with F71 and numerous alkyl-aryl interactions with surrounding hydrophilic amino acid side chains flanking the lower section of the deeper subpocket (**Fig. 5- C, D**). Thus, our experimental results corelates well with docking studies indicative of possible Bcl-2 inhibition potential of **S2**.

2.8 PPARγ transactivation assay

Compounds **S1-S13**, containing a pyrrolidine-2,5-dione moiety which resembles the thiazolidinedione ring of PPARγ agonists Rosiglitazone and Pioglitazone, were evaluated for both agonist and antagonist activity on the human PPARγ (hPPARγ) subtype to ascertain effects of bio isosteric replacement of TZD ring with pyrrolidine-2,5-dione, at binding site of PPARγ. For this purpose, GAL-4 PPARγ chimeric receptor was expressed in transiently transfected HepG2 cells according to a previously reported procedure[47][48]. The agonist activity of these compounds was evaluated at three concentrations (1 μM, 5 μM and 25 μM) and compared with that of the corresponding reference agonist Pioglitazone, but no significant activity was observed for all compounds (Supporting data, **Supporting Fig. S1**). To rule out any potential bond with the receptor, we also evaluated a possible antagonist activity by conducting a competitive binding assay in which PPARγ activity at a fixed concentration of the reference agonist Pioglitazone (2 μM) was measured in cells treated with increasing concentrations of representative compounds **S1-S7**, but also in this case we did not observe any significant activity (Supporting data, **Supporting Fig. S2**). Thus, this series of compounds do not interact with PPARγ receptor as agonists or antagonists, and antitumor effects exhibited are independent of PPARγ.

2.9 HDAC activity assay

Pyrazoline ring has been identified as an appropriate surface recognition motif in designing of HDAC inhibitors [49]–[51], to ascertain HDAC inhibitory potential, we undertook preliminary HDAC screening of **S1-S13** on two isoforms of HDACs, HDAC 4 (Class II HDAC) and HDAC 8 (Class I HDAC) belonging to two different HDAC classes. A single dose of 50 μM of each test compound was used in preliminary screening, and residual

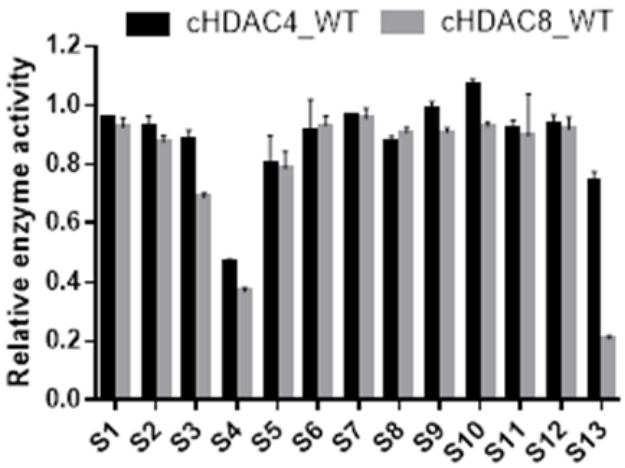

Figure 6. Percent relative activity of HDAC4 and HDAC8 after treatment with S1-S13 at 50 μM concentration. n = 3, values are presented as Mean and error bars represents standard error of mean.

percentage HDAC activity observed is presented in **Fig. 6** and details have been presented in Supplementary data**, Supplementary Tables-ST1** and **ST2**. For HDAC4, the relative HDAC activity after treatment with all compounds, was >0.6 (60%) hence IC_{50} values were not determined for any of the compounds as high HDAC4 activity was retained. Only **S4** and **S13** showed higher activities and were taken forward to determine IC_{50} values. The IC_{50} values for **S4** were >50 μM against HDAC4 and 24.9μM against HDAC8, respectively, while **S13** turned out to be to have IC_{50} values >50 μM on both HDAC isoenzymes. Thus, our results indicate that this series of compounds is presently does not exhibit significant HDAC inhibition but could be modified extensively further possibly to obtain class I HDAC inhibitors. Details of experimental method are included in Supplementary data.

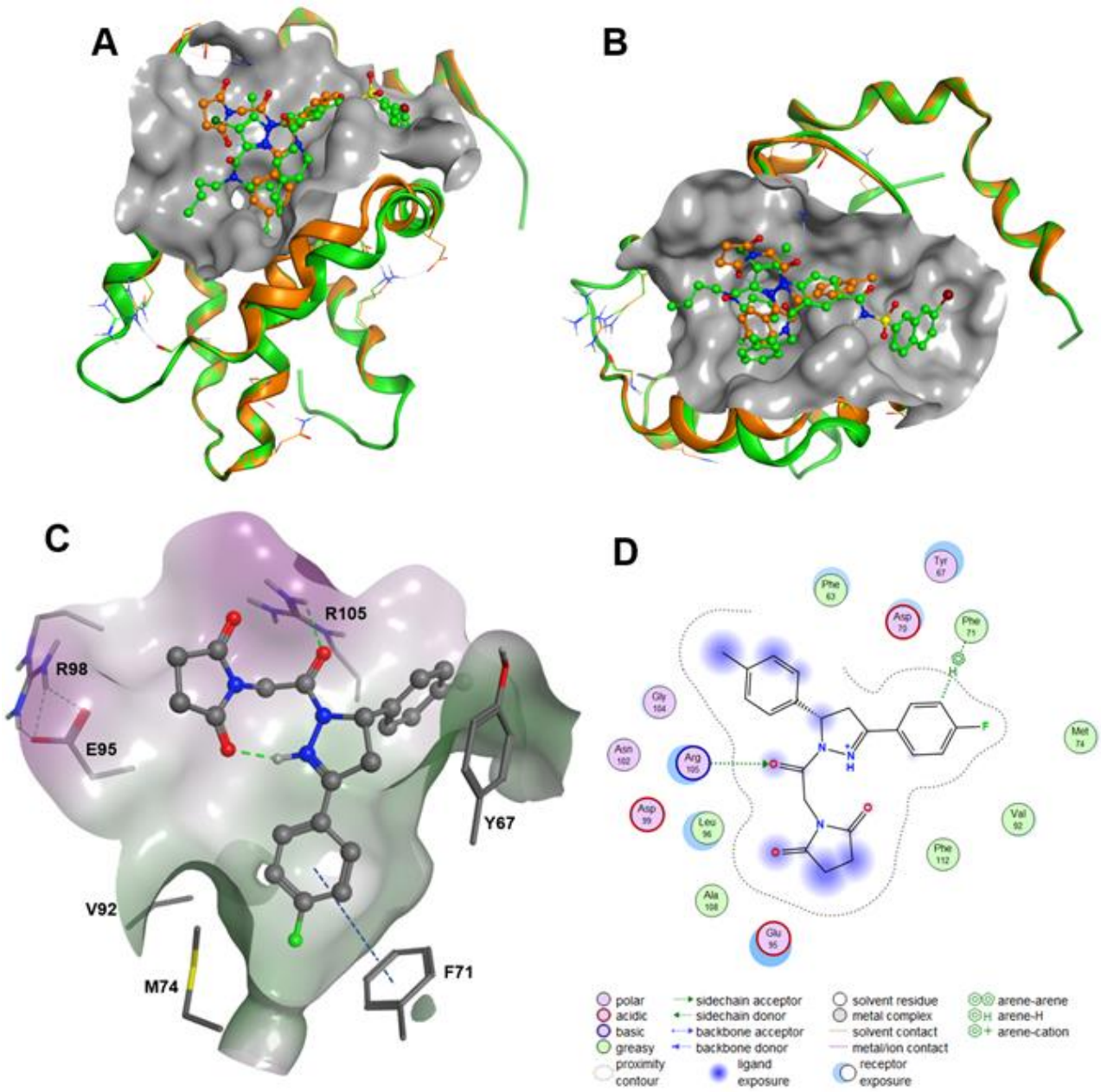

Figure 5. Binding poses of small molecule BH3 mimetics within the binding groove of Bcl-2. A) Sideview and B) Top view of superposed crystal structures of Bcl-2 (PDB-ID 4AQ3 (F-chain) in complex with its native ligand (green) and docked to R-S2 (orange). Surface of binding site is shown in gray. C) Site view of best binding pose of R-S2 within the deep main pocket of Bcl-2. Hydrogen bonds are shown as green dashed lines. The dashed dark blue line denotes an edge-to-face Pi-interactions between F71 and one phenyl rings of R-S2. The transparent surface of the binding site varies from hydrophobic (green) to polar (magenta). D) 2D protein-ligand interactions. Green dashed arrow denotes the key hydrogen bond to R105.

2.8 *In vivo* tumor regression in HT29 xenografts

Various literature reports revealed the in vivo efficacy of diaryl pyrazoline derivatives[52]–[54], but to the best of our knowledge, there were no reports found about the in vivo antitumor efficacy of pyrrolidine-2,5-diones, hence it was of interest to pursue the in vivo effects of these novel diaryl pyrazoline and pyrrolidine-2,5-dione hybrids in tumor xenografts. Pre-clinical toxicology studies in mice permits for optimization of treatment cycles as well as identification of safe starting doses and potential human toxicity. Therefore, first acute toxicity study was carried out which determined maximum non-toxic single dose of compound S2, as 100 mg/kg (details in supplementary data) and half of this dose was selected for efficacy study. None of the animals showed the changes in behavioral or physical activity. Also, no significant changes were observed in weight of the treated animals as compared to control group. The autopsy of the animals revealed no visible changes in the organs such as liver, heart and spleen

and tissue damage. Anticancer effect of **S2** was evaluated in HT-29 colorectal adenocarcinoma xenografts in Balb/c nude mice. Male Balb/c nude mice 6–8 weeks of age were obtained from N.N. Blokhin Cancer Research Center. The mice were housed in a pathogen-free environment under controlled conditions of light and humidity and received food and water ad libitum. HT-29 cells (5×10^6) were implanted subcutaneously with Matrigel® (1:1; Matrix) into left flank of mice. Once the mean tumor volume reached ~65 mm^3, animals were randomized into treatment groups (n=6–10), and dosing with **S2** was initiated (day 1): 50 mg/kg i.p. (intraperitoneally) or *per os (orally)* daily during 20 days (cumulative dose 1 g/kg).Tumor sizes and body weights were measured twice weekly. Tumor volume was calculated by the formula: $V=\pi/6*(L*W*H)$, where L is length, W is width and H is height of tumor. Efficiency assessment was carried out using TGI (tumor growth inhibition). Statistical analyses of *in vivo* research were performed using SPSS V. 22.0 comparing continuous variables by non-parametrical Mann-Whitney U. Data are expressed as mean ± standard deviation (SD). Effect of **S2** on tumor progression in HT-29 xenografts is presented in **fig. 7**. **S2** demonstrated significant antitumor effect after both i.p. and *per os* (oral route) administration. On day 12 of treatment, maximum TGI 66 and 60% was observed with average tumor volume 167.7±28.6 mm^3 (p=0.002) and 193.1±15.2 mm^3 (p=0.002) vs 488.0±95.7 mm^3 in **S2** i.p., **S2** *per os* (orally) and control groups, respectively. On next day after the end of treatment (day 21) TGI 49 and 48% were detected, no significant differences between i.p. and *per os* groups were observed. Statistical analysis revealed the significant differences between the group receiving compound S2 and the control group (details in supplementary data, **Supplementary Table ST5 to ST7**), suggesting that **S2** has good availability when absorbed from the gastrointestinal tract. Moreover, in the mice group treated with S2, no significant body weight loss and no evident toxic signs in liver and spleen were observed.

3. Conclusion

In conclusion, a series of novel pyrazoline-substituted pyrrolidine-2,5-diones were synthesized. As both pyrazoline and pyrrolidine-2,5-dione moieties are present in numerous antiproliferative molecules, all the derivatives were screened to determine their *in vitro* cytotoxic activity against three human tumor cell lines, namely MCF7, HT29, and K562. The results showed that most compounds displayed excellent cytotoxic activities towards MCF-7 and HT29 cells and moderate effects on K562 cells. Compounds **S2**, **S6**, **S7**, and **S13** were found to be the most effective antiproliferative agents. Particularly, **S2** was found to be the most potent, on MCF7 and HT29 with IC_{50} values 0.78 µM and 0.92 µM, respectively. **S2** also caused disruption in cell cycle phases leading to decreased population of cells in G2/M phase and increased cell population in G0/G1 phase. The excellent antiproliferative effects of **S2** can be correlated with the dose dependent inhibition of anti-apoptotic protein Bcl-2 and experimental results found to corelate well with docking studies. Even with the similar structural features to PPARγ and HDAC inhibitors, current series of compounds does not affect both the targets, and thus antitumor effects can be attributed to targeting of Bcl-2. **S2**, also, exhibited equivalent and promising *in vivo* tumor regression by both i.p. and oral route in nude mice, indicating bioavailability and anti-tumor efficacy through GI absorption post oral administration. Apart from the oral bioavailability, the fact that **S2** did not induce any toxic effects in vivo, strongly supports the potential of this molecule as a lead for further considerations. Thus, our finding about the in vivo antitumor efficacy of pyrrolidine-2,5-dione derivatives is kind of amongst first few prototype examples and thus, the significant contribution to the scientific community. The *in-silico* studies indicated desirable physicochemical and pharmacokinetic properties of molecules making the drug like molecules. Thus, our current results advocate that this series of compounds holds promise for the development of more potent, less toxic and specific anticancer agents.

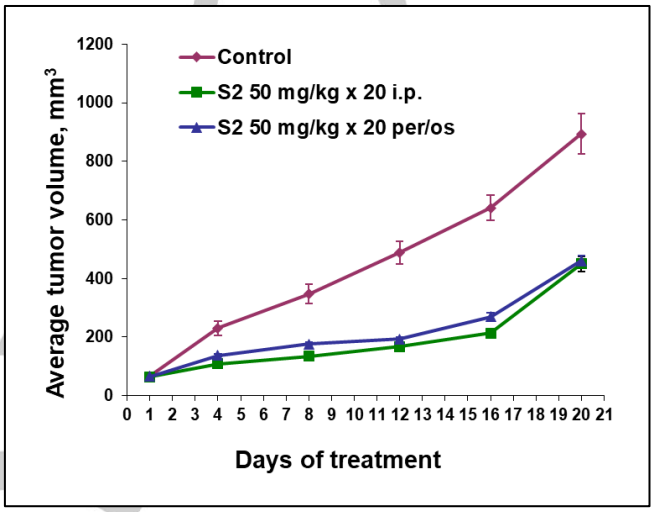

Figure 7. Tumor regression by S2 in HT29 xenografts. Graph of tumor volume vs. time in HT29 xenografts treated with S2, 50 mg/kg i.p. (rectangle), **S2,** 50 mg/kg *per os*. (up triangle), and saline i.p. control (diamond). Error bars represent SEM, n=6. p<0.002.

4. Material and Methods

4.1 Chemistry

Commercial Grade reagents of make S D Fine, Sigma Aldrich or Research Lab were acquired from dealers in India. Thin layer chromatography (TLC) was done on pre-coated Merck Silica Gel 60 F254. Melting points were determined by open capillary method using VEEGO melting point device and are uncorrected. Infrared (FTIR) spectra were obtained using Schimadzu FT/IR-8400S with use of direct sampling technique. ^1H and ^{13}C NMR spectra were recorded on a Bruker instrument at 400 MHz, TMS as internal standard and chemical shift values (δ) are described in ppm. J values (Coupling constants) are stated in hertz (Hz). Abbreviations in NMR interpretation are, s- singlet, d-doublet, dd - doublet of doublet, t-triplet, m- multiplet, and q - quartet. Mass spectrums were recorded with LC-MS Agilent Technologies 1260 Infinity instrument. The percentage purity (≥95 %) of final products S1-S13, were established by using HPLC (high-performance liquid chromatography) Agilent 1100 instrument. The conditions of HPLC chromatography: column - Hemochrome C18 (15cm), detector- UV visible detector, detection wavelength- 300 nm, flow rate-1mL/min, sample concentration- 10 ppm, oven temperature - 30 °C; technique - gradient elution with a run time of 15 min using

mobile phase consisting of Methanol: Formic acid (0.1%) in 70:30 ratio.

4.2 Synthesis

4.2.1 Synthetic procedure for A1-A13

Various chalcones were prepared as reported previously. Briefly, A solution of **1** (acetophenone or 4-Flouroacetophenone or 2,4-Diflouroacetophenone) and **2** (variously substituted aldehydes)**,** in equimolar proportion, were stirred in hydroalcoholic solution of sodium hydroxide in cold conditions. The solid obtained was filtered at pump and recrystallized from ethanol to obtain chalcones, **A1-A13**.

1-phenyl-3-(p-tolyl)prop-2-en-1-one (A1) Yellow crystals. Yield 6.8 g (83%). M.P. 88-89 °C. FTIR (cm^{-1}) 3057, 3022, 2912, 1656, 1591, 1566. ^{1}H-NMR (400 MHz, $CDCl_3$) δ ppm 2.39 (s, 3H), 7.13–7.18 (m, 2H), 7.19 – 7.26 (m, 3H), 7.53 – 7.55 (m, 2H), 7.78 (s, 1H), 7.81 (s, 1H), 8.02 – 8.07 (m, 2H).

1-(4-fluorophenyl)-3-(p-tolyl)prop-2-en-1-one (A2). Yellow crystals. Yield 8.4 g (80%). M.P. 140.5-141 °C. FTIR (cm^{-1}) 3074, 2918, 1660, 1593, 1523, 1215. ^{1}H-NMR (400 MHz, $CDCl_3$) δ ppm 2.39 (s, 3H), 7.15 – 7.19 (m, 2H), 7.22 – 7.26 (m, 2H), 7.47 (s, 1H), 7.53 – 7.55 (m, 2H), 7.77 (s, 1H), 8.03 – 8.07 (m, 2H).

1-(2,4-difluorophenyl)-3-(p-tolyl)prop-2-en-1-one (A3). Yellow crystals. Yield 7 g (80%). M.P. 66-68 °C. FTIR (cm^{-1}) 3302, 2902, 1662, 1595, 1568, 1286, 1265, 1234. ^{1}H-NMR (400 MHz, $CDCl_3$) δ ppm 2.35 (s, 3H), 7.14 – 7.19 (m, 2H), 7.23 – 7.27 (m, 2H), 7.48 (s, 1H), 7.53 – 7.55 (m, 1H), 7.77 – 7.81 (m, 1H), 8.03 – 8.07 (m, 2H).

1-(2,4-difluorophenyl)-3-(furan-2-yl)prop-2-en-1-one (A4). Yellow crystals. Yield 8.8 g (89%). M.P. 67-68 °C. FTIR (cm^{-1}) 3078, 1668, 1545, 1251, 1234. ^{1}H-NMR (400 MHz, $CDCl_3$) δ ppm 6.51–6.52 (m, 1H), 6.74 (d, J=3.4 Hz, 1H), 6.96–7.01 (m, 1H), 7.29 (m, 1H), 7.57 (t, J=7.6 Hz, 2H), 7.86–7.92 (m, 1H).

3-(2-chlorophenyl)-1-phenylprop-2-en-1-one (A5). Pale yellow crystals. Yield 5 g (88%). M.P. 67-68 °C. FTIR (cm^{-1}) 3074, 1664, 1579, 686. ^{1}H-NMR (400 MHz, $CDCl_3$) δ ppm 6.97 – 7.01 (m, 1H), 7.09 – 7.13 (m, 1H), 7.57 – 7.60 (m, 2H), 7.61 – 7.65 (m, 3H), 7.76 – 7.79 (m, 1H), 8.03 – 8.17 (m, 3H).

Chalcone (A6)
Yellow shiny crystals. Yield 7 g (93%). M.P. 56-58 °C. FTIR (cm^{-1}) 3084, 3053, 1660, 1573. ^{1}H-NMR (400 MHz, $CDCl_3$) δ ppm 7.35–7.37 (m, 3H), 7.40–7.49 (m, 2H), 7.51–7.55 (m, 2H), 7.58–7.61 (m, 2H), 7.78 (d, J=15.7 Hz, 1H), 7.99 (q, 2H).

3-(4-fluorophenyl)-1-phenylprop-2-en-1-one **(A7).** Yellow crystals. Yield 7 g (87%). M.P. 65-66 °C. FTIR (cm^{-1}) 3078, 1662, 1575, 1321. ^{1}H-NMR (400 MHz, $CDCl_3$) δ ppm 7.09 – 7.13 (m, 2H), 7.48 – 7.52 (m, 3H), 7.57 – 7.60 (m, 1H), 7.61 – 7.65 (m, 3H), 8.00 – 8.02 (m, 2H).

1-(4-fluorophenyl)-3-phenylprop-2-en-1-one (A8). Yellow crystals. Yield 5 g (61%). M.P. 73-74 °C. FTIR (cm^{-1}) 3059, 1658, 1585, 1209 ^{1}H-NMR (400 MHz, $CDCl_3$) δ ppm 7.14–7.19 (m, 2H), 7.39–7.42 (m, 3H), 7.50 (d, J=15.6 Hz, 1H), 7.62–7.64 (m, 2H), 7.81 (d, J=15.6 Hz, 1H), 8.03–8.07 (m, 2H).

1-phenyl-3-(thiophen-2-yl)prop-2-en-1-one (A9). Yellow crystals. Yield 6.9 g (82%). M.P. 68-70 °C. FTIR (cm^{-1}) 3107, 3066, 1660, 1597, 1552. ^{1}H-NMR (400 MHz, $CDCl_3$) δ ppm 7.44 – 7.46 (m, 2H), 7.60 – 7.64 (m, 2H), 7.67 (s, 1H), 7.84 (s, 1H), 7.92 – 7.93 (m, 1H), 8.03 – 8.07 (m, 2H), 8.42 – 8.43 (m, 1H).

3-(furan-2-yl)-1-phenylprop-2-en-1-one (A10). Pale yellow crystals. Yield 5.6 g (85%). M.P. 72-74 °C. FTIR (cm^{-1}) 3107, 3066, 1660, 1597. ^{1}H-NMR (400 MHz, $CDCl_3$) δ ppm 7.15 – 7.21 (m, 2H), 7.29 – 7.33 (m, 1H), 7.44 (s, 1H), 7.46 (s, 1H), 7.66 – 7.68 (m, 1H), 8.03 – 8.06 (m, 2H), 8.07 – 8.11 (m, 2H).

1-(4-fluorophenyl)-3-(furan-2-yl)prop-2-en-1-one (A11). Yellow crystals. Yield 8.6 g (88%). M.P. 100-101 °C. FTIR (cm^{-1}) 3109, 3066, 1658, 1597, 1587, 1217. ^{1}H-NMR (400 MHz, $CDCl_3$) δ ppm 6.50–6.51 (m, 1H), 6.71 (d, 1H), 7.13–7.18 (m, 2H), 7.42 (d, J=15.3 Hz, 1 H), 7.52 (d, 1H), 7.59 (d, J=15.3 Hz, 1H), 8.04–8.08 (m, 2H).

1-(2,4-difluorophenyl)-3-(3,4-dimethoxyphenyl)prop-2-en-1-one (A12). Off-white colour solid. Yield 5.6 g (78 %). M.P. 111-113 °C. FTIR (cm^{-1}) 3072, 2843, 1654, 1591, 1508, 1220. ^{1}H-NMR (400 MHz, $CDCl_3$) δ ppm 3.93 (s, 6H), 6.87 – 6.93 (m, 2H), 6.96 – 7.01 (m, 1H), 7.13 (m, 1H), 7.20 – 7.23 (m, 2H), 7.69-7.73 (m, 1H), 7.84 – 7.90 (m, 1H).

3-(3,4-dichlorophenyl)-1-phenylprop-2-en-1-one (A13). Yellow crystals. Yield 6.7 g (83%). M.P. 140-142 °C. FTIR (cm^{-1}) 3169, 3043, 1664, 1579, 688. ^{1}H-NMR (400 MHz, $CDCl_3$) δ ppm 6.86 – 6.97 (m, 2H), 7.49 – 7.53 (m, 2H), 7.57 – 7.58 (m, 1H), 7.59 – 7.66 (m, 2H), 7.82 (s, 1H), 8.00 – 8.03 (m, 2H).

4.2.2 Synthetic procedure for B1-B13

A1-A13 (5g, 0.02mol) were dissolved in chloroform and hydrazine hydrate (2.5mL, 0.04mol) was added dropwise. The reaction mixture was refluxed at 80°C for 12h. The reaction mixture was then cooled to the room temperature and K_2CO_3 (8g, 0.05mol) was added and stirred for 15min in ice bath. To this ice-cold solution chloroacetyl chloride (4mL, 0.03mol) was added dropwise using dropping funnel and stirred for 12h at room temperature. Chloroform layer was washed with water and evaporated under vacuum. Crude solid was purified by extracting with diethyl ether to get white solid of intermediates **B1-B13.**

2-chloro-1-(3-phenyl-5-(p-tolyl)-4,5-dihydro-1H-pyrazol-1-yl)ethanone (B1). Cream colour solid. Yield 5.3 g (52%). M.P. 117-118 °C. FTIR (cm^{-1}) 2951, 1666, 1599, 1514, 1489, 1429, 688. ^{1}H-NMR (400 MHz, $CDCl_3$) δ ppm 2.31 (s, 3H), 3.21 (dd, J=17.8 Hz, 1H), 3.73-3.80 (m, 1H), 4.57 (m, 2H), 5.56 (dd, J=11.8 Hz, 1H), 7.13 (s, 4H), 7.43-7.46 (m, 3H), 7.74-7.76 (m, 2H).

2-chloro-1-(3-(4-fluorophenyl)-5-(p-tolyl)-4,5-dihydro-1H-pyrazol-1-yl)ethanone (B2). Off white colour. Yield 4.8 g (56%). M.P. 119-121°C. FTIR (cm^{-1}) 2835, 1649, 1602, 1512, 1236, 831. ^{1}H-NMR (400 MHz, $CDCl_3$) δ ppm 3.20 (dd, J=17.8 Hz, 1H), 3.70-3.74 (m, 1H), 3.77 (s, 3H), 4.54 (s, 2H), 5.55 (dd, J=11.8 Hz, 1H), 6.83-6.86 (m, 2H), 7.10-7.18 (m, 4H), 7.73-7.77 (m, 2H).

2-chloro-1-(3-(2,4-difluorophenyl)-5-(p-tolyl)-4,5-dihydro-1H-pyrazol-1-yl)ethanone (B3). White colour. Yield 5 g (67%). M.P. 120-122 °C. FTIR (cm^{-1}) 1681, 1600, 1514, 1502, 1257, 1207, 813. ^{1}H-NMR (400 MHz, $CDCl_3$) δ ppm 2.31 (s, 3H), 3.27 – 3.33 (m, 1H), 3.80 – 3.88 (m, 1H), 4.49– 4.56 (m, 2H), 5.53 (dd, J=11.6 Hz, 1H), 6.84 – 6.90 (m, 1H), 6.95 – 7.00 (m, 1H), 7.11 – 7.15 (m, 4H), 7.95 – 8.01 (m, 1H).

2-chloro-1-(3-(2,4-difluorophenyl)-5-(furan-2-yl)-4,5-dihydro-1H-pyrazol-1-yl)ethanone (S4). Cream colour. Yield 4.5 g (51%). M.P. 109.5-110.5 °C. FTIR (cm^{-1}) 1672, 1602, 1494, 1263, 1217, 783. ^{1}H-NMR (400 MHz, $CDCl_3$) δ ppm 3.55–3.61 (m, 1H), 3.66–3.74 (m, 1H), 4.52 (q, 2H), 5.67 (m, 1H), 6.32 (q, 1H), 6.39 (d, J=3.2 Hz, 1H), 6.86–6.94 (m, 1H), 6.95-7.00 (m, 1H), 7.31 (t, J=0.86 Hz, 1H), 7.95–8.01 (m, 1H).

2-chloro-1-(5-(2-chlorophenyl)-3-phenyl-4,5-dihydro-1H-pyrazol-1-yl)ethanone (B5). White colour solid. Yield 5.2 g (56%). M.P. 151-152 °C. FTIR (cm^{-1}) 1672, 1593, 1566, 758. ^{1}H-NMR (400 MHz, $CDCl_3$) δ ppm 3.13 (dd, J=17.8 Hz, 1H), 3.84-3.92 (m, 1H), 4.60 (q, 2H), 5.91-5.95 (m, 1H), 7.08–7.12 (m, 1H), 7.20–7.26 (m, 2H), 7.39–7.45 (m, 4H), 7.72–7.75 (m, 2H).

2-chloro-1-(3,5-diphenyl-4,5-dihydro-1H-pyrazol-1-yl)ethanone (B6). White colour solid. Yield 4.6 g (51%). M.P. 117-118 °C. FTIR (cm^{-1}) 2955, 1660, 1597, 1568, 1542, 1521, 756. ^{1}H-NMR (400 MHz, $CDCl_3$) δ ppm 3.20 (dd, J=17.8 Hz, 1H), 3.75 (dd, J=17.8 Hz, 1H), 4.57 (q, 2H), 5.57 (dd, J=11.7 Hz, 1H), 7.22–7.27 (m, 3H), 7.29–7.33 (m, 2H), 7.40–7.45 (m, 3H), 7.72–7.75 (m, 3H).

2-chloro-1-(5-(4-fluorophenyl)-3-phenyl-4,5-dihydro-1H-pyrazol-1-yl)ethanone (B7). Buff white colour solid. Yield 5 g (57%). M.P. 119-121 °C. FTIR (cm^{-1}) 1656, 1602, 1509, 1330, 719. ^{1}H-NMR (400 MHz, $CDCl_3$) δ ppm 3.20 (dd, J=18 Hz, 1H), 3.75-3.83 (m, 1H), 4.52-4.61 (m, 2H), 5.57 (dd, J=11.6 Hz, 1H), 6.99-7.04 (m, 2H), 7.21-7.26 (m, 2H), 7.42-7.49 (m, 3H), 7.74-7.76 (m, 2H).

2-chloro-1-(3-(4-fluorophenyl)-5-phenyl-4,5-dihydro-1H-pyrazol-1-yl)ethanone (B8). Off white colour solid. Yield 4.9 g (53%). M.P. 125-12 7 °C. FTIR (cm^{-1}) 1678, 1600, 1514, 1494, 1217, 696. ^{1}H-NMR (400 MHz, $CDCl_3$) δ ppm 3.20 (dd, J=17.6 Hz, 1H), 3.73-3.80 (m, 1H), 4.52-4.59 (m, 2H), 5.60 (dd, J=11.6 Hz, 1H), 7.10 – 7.15 (m, 2H), 7.21 – 7.25 (m, 2H), 7.26 – 7.29 (m, 1H), 7.31 – 7.35 (m, 2H), 7.72-7.77 (m, 2H).

2-chloro-1-(3-phenyl-5-(thiophen-2-yl)-4,5-dihydro-1H-pyrazol-1-yl)ethanone (B9). White colour solid. Yield 6.1 g (62%). M.P. 120-122 °C. FTIR (cm^{-1}) 1658, 1580, 1500, 1437, 1423, 690. ^{1}H-NMR (400 MHz, $CDCl_3$) δ ppm 3.41 (dd, J= 17.8 Hz, 1H), 3.72-3.80 (m, 1H), 4.52-2.49 (m, 2H), 5.92 (dd, J=11.2 Hz, 1H), 6.92-6.94 (m, 1H), 7.06-7.07 (m, 1H), 7.19-7.20 (m, 1H), 7.42-7.49 (m, 3H), 7.75-7.77 (m, 2H).

2-chloro-1-(5-(furan-2-yl)-3-phenyl-4,5-dihydro-1H-pyrazol-1-yl)ethanone (B10). White colour solid. Yield 5.8 g (60%). M.P. 138-140 °C. FTIR (cm^{-1}) 1664, 1595, 1566, 759. ^{1}H-NMR (400 MHz, $CDCl_3$) δ ppm 3.49-3.65 (m, 2H), 4.51-4.60 (m, 2H), 5.68-5.72 (m, 1H), 6.31-6.33 (m, 1H), 6.39-6.40 (m, 1H), 7.26-7.30 (m, 1H), 7.42-7.49 (m, 3H), 7.75-7.78 (m, 2H).

2-chloro-1-(3-(4-fluorophenyl)-5-(furan-2-yl)-4,5-dihydro-1H-pyrazol-1-yl)ethanone (B11). Grey colour. Yield 6.9g (78.5%). M.P. 139-141 °C. FTIR (cm^{-1}) 1672, 1600, 1514, 1487, 1222, 808. ^{1}H-NMR (400 MHz, $CDCl_3$) δ ppm 3.47 (dd, J=17.6 Hz, 1H), 3.60 (dd, J=17.6 Hz, 1H), 4.52 (q, 2H), 5.68 (dd, J=11.5 Hz, 1H), 6.30 (q, 1H), 6.37 (d, J=3.2 Hz, 1H), 7.10–7.15 (m, 2H), 7.29 (t, J=3.7 Hz, 1H), 7.73–7.77 (m, 2H).

2-chloro-1-(3-(2,4-difluorophenyl)-5-(3,4-dimethoxyphenyl)-4,5-dihydro-1H-pyrazol-1-yl)ethanone (B12). Off-white colour solid. Yield 5 g (74 %). M.P.145-148 °C. FTIR (cm^{-1}) 3076, 3007, 2939, 1670, 1604, 1514, 1464, 1253, 1234, 846. ^{1}H-NMR (400 MHz, $CDCl_3$) δ ppm 3.29 – 3.35 (m, 1H), 3.79 – 3.88 (m, 7H), 4.45– 4.59 (m, 2H), 5.52 (dd, J=11.6Hz, 1H), 6.76 – 6.83 (m, 3H), 6.85 – 6.91 (m, 1H), 6.95 – 7.00 (m, 1H), 7.95 – 8.01 (m, 1H).

2-chloro-1-(5-(3,4-dichlorophenyl)-3-phenyl-4,5-dihydro-1H-pyrazol-1-yl)ethanone(B13). Off white colour solid. Yield 5.4 g (50%). M.P. 159-161 °C. FTIR (cm^{-1}) 1681, 1668, 1600, 1568, 1541, 783. ^{1}H-NMR (400 MHz, $CDCl_3$) δ ppm 3.17-3.23 (m, 1H), 3.76-3.84 (m, 1H), 4.52-4.64 (m, 2H), 5.74 (dd, J=12 Hz, 1H), 6.79-6.86 (m, 2H), 7.14-7.18 (m, 1H), 7.41-7.48 (m, 3H), 7.49-7.73 (m, 2H).

4.2.3 Synthetic procedure for derivatives S1-S13

Finally, the intermediates **B1-B13** (1g, 0.01 mol) were condensed with pyrrolidine-2,5-dione, **3** (1g, 0.03-0.04 mol), in the presence of mild base potassium hydroxide (2.5 g, 0.03 moles) in DMF by stirring at room temperature for 6-12 hrs. The crude product was precipitated by adding water to the reaction mixture, which was filtered at pump, washed with water and recrystallized either from ethanol, chloroform or (3:1) combination of methanol and chloroform to obtain white needle shaped crystals of **S1-S13**.

1-(2-oxo-2-(3-phenyl-5-(p-tolyl)-4,5-dihydro-1H-pyrazol-1-yl)ethyl)pyrrolidine-2,5-dione (S1) Yield 1.25 g (62.5%); M.P. 148.1°C; White crystalline solid; IR (cm^{-1}) 2866, 1705, 1674, 1602; ^{1}H NMR (400 MHz, DMSO-d_6, δ ppm) 2.28(s, 3H), 2.74(s, 4H), 3.11-3.27 (dd, J = 18.4 Hz, 1H), 3.69-3.76 (m, 1H), 4.67-4.71(d, J = 16 Hz, 1H), 4.83-4.87(d, J = 16 Hz, 1H), 5.48-5.52 (dd, J = 11.6 Hz, 1H), 7.08-7.14 (m, 6H), 7.71-7.74 (m, 3H); ^{13}C NMR (400 MHz, DMSO-d_6) 20.57, 27.97, 42.00, 59.53, 115.7-138.6, 155, 177, 162.7, 162.19; UV Spectrum (10 ppm) λ_{max} 299.2 nm; Theoretical mass 375.4, LC-MS (m/z, I %), 376.2 [$(M+H)^+$, 100%]; HPLC Purity % Area 99.3 %, RT 6.52 mins.

1-(2-(3-(4-fluorophenyl)-5-(p-tolyl)-4,5-dihydro-1H-pyrazol-1-yl)-2-oxoethyl)pyrrolidine-2,5-dione (S2) Yield 1.11 g (55.5%); M.P. 203°C; White crystalline solid; IR (cm^{-1}) 2903, 1703, 1660, 1600, 1153; ^{1}H NMR (400 MHz, DMSO-d_6, δ ppm) 2.26(s, 3H), 2.70(s, 4H), 3.14-3.19(dd, J = 18.4 Hz, 1H), 3.84-3.91(m, 1H), 4.67-4.71(q, J = 15.2 Hz, 2H), 5.47-5.51(dd, J = 11.6 Hz, 1H), 7.07-7.14 (m, 4H), 7.30-7.35(t, J = 8.8 Hz, 2H), 7.87-7.90(m, 2H); ^{13}C NMR (400 MHz, DMSO-d_6) 20.57, 27.97, 42.00, 5 9.53, 115.7-138.6, 155, 177,162.7, 162.19; UV Spectrum (10ppm) λ_{max} 289.9 nm; Theoretical mass 393.1, LC-MS (m/z, I %), 394.1 [$(M+H)^+$, 100%]; HPLC Purity % Area 99.15 %, RT 8.71 mins.

1-(2-(3-(2,4-difluorophenyl)-5-(p-tolyl)-4,5-dihydro-1H-pyrazol-1-yl)-2-oxoethyl)pyrrolidine-2,5-dione (S3) Yield 1.3 g (65%); M.P. 181.6°C; White crystalline solid; IR (cm^{-1}) 2921, 1707, 1676, 1599, 1168; ^{1}H NMR (400 MHz, DMSO-d_6, δ ppm) 2.27(s, 3H), 2.71(s, 4H), 3.16-3.17(dd, J = 18.4 Hz, 1H), 3.90-3.97(m, 1H), 4.52-4.64(q, J = 16.4 Hz, 2H), 5.46-5.50(dd, J = 11.8 Hz, 1H), 7.08-7.16 (m, 4H), 7.18-7.20(m, 1H), 7.27-7.32(m, 1H), 7.80-7.97(m, 1H); ^{13}C NMR (400 MHz, DMSO-d_6) 20.58, 27.95, 43.93-43.98, 59.58, 104.66-138.39, 151.7-151.27, 176.89, 162.87, 162.12; UV Spectrum (10ppm) λ_{max} 287.1 nm; Theoretical mass 411.1, LC-MS (m/z, I %), 412.1 [$(M+H)^+$, 100%]; HPLC Purity % Area 96.81 %, RT 8.04 mins.

1-(2-(3-(2,4-difluorophenyl)-5-(furan-2-yl)-4,5-dihydro-1H-pyrazol-1-yl)-2-oxoethyl)pyrrolidine-2,5-dione (S4) Yield 1.15 g (57.5%); M.P. 149.8°C; White crystalline solid; IR (cm^{-1}) 2929, 1705, 1660, 1602, 1157; ^{1}H NMR (400 MHz, DMSO-d_6, δ ppm) 2.73(s, 4H), 3.80-3.87(m, 1H), 3.90-3.97(m, 2H), 5.61-5.65(dd, J = 11.8 Hz, 1H), 6.33(d, J = 2.8, 1H), 6.39(d, J = 1.6, 1H), 7.21-7.26 (m, 1H), 7.38-7.44(m, 1H), 7.57(s, 1H), 7.97-8.08(m, 1H); ^{13}C NMR (400 MHz, DMSO-d_6) 27.98, 40.05, 53.35, 104.87-142.64, 151.55-151.70, 177.15, 163.03; UV Spectrum (10ppm) λ_{max} 285.5nm; Theoretical mass 387.1, LC-MS (m/z, I %), 388 [$(M+H)^+$, 100%]; HPLC Purity % Area 98.44 %, RT 4.56 mins.

1-(2-(5-(2-chlorophenyl)-3-phenyl-4,5-dihydro-1H-pyrazol-1-yl)-2-oxoethyl)pyrrolidine-2,5-dione (S5) Yield 1.22 g (61 %); M.P. 222.6 °C; White crystalline solid; IR (cm^{-1}) 2820, 1703, 1676, 1601, 692; ^{1}H NMR (400 MHz, DMSO-d_6, δ ppm) 2.70(s, 4H), 3.10-3.16 (dd, J = 18 Hz, 1H), 3.97-4.05 (m, 1H), 4.56-4.60 (d, J = 16.8 Hz, 1H), 4.69-4.73(d, J = 17.2 Hz, 1H), 5.75-5.79 (dd, J = 12 Hz, 1H), 7.11-7.83 (m, 9H); ^{13}C NMR (400 MHz, DMSO-d_6): 27.99, 42.92, 57.86, 129.59-130.85, 156.05, 177.11, 162.99, 129.69; UV Spectrum (10ppm) λ_{max} 288.3 nm; Theoretical mass 395.1, LC-MS (m/z, I %), 396.1 [$(M+H)^+$, 100%]; HPLC Purity % Area 98.14 %, RT 7.20 mins.

1-(2-(3,5-diphenyl-4,5-dihydro-1H-pyrazol-1-yl)-2-oxoethyl)pyrrolidine-2,5-dione (S6) Yield 0.9 g (45 %); M.P. 201.1 °C; White crystalline solid; IR (cm^{-1}) 2951, 1707, 1674, 1601; ^{1}H NMR (400 MHz, DMSO-d_6, δ ppm) 2.71(s, 4H), 3.16-3.21 (dd, J = 18.2 Hz, 1H), 3.88-3.95(m, 1H), 4.54-4.68 (q, J = 18.1 Hz, 2H), 5.52-5.56(dd, J = 11.2 Hz, 1H), 7.19-7.84 (m, 10H); ^{13}C NMR (400 MHz, DMSO-d_6) 27.99, 42.92, 57.86, 129.59-130.85, 156.05, 177.11, 162.99, 129.69; UV- Spectrum (10ppm)λ_{max} 290nm; Theoretical mass 361.1, LC-MS (m/z, I %), 362.1 [$(M+H)^+$, 100%]; HPLC Purity % Area 98.59 %, RT 5.11 mins.

1-(2-(5-(4-fluorophenyl)-3-phenyl-4,5-dihydro-1H-pyrazol-1-yl)-2-oxoethyl)pyrrolidine-2,5-dione Yield 0.99g (49.5 %); M.P. 181.1°C; White crystalline solid; IR (cm^{-1}) 2903, 1701, 1674, 1602; ^{1}H NMR (400 MHz, DMSO-d_6, δ ppm) 2.71(s, 4H), 3.18-3.23(dd, J = 11.6 Hz, 1H), 3.90-3.95 (m, 1H), 4.53-4.66(q, J = 16.9 Hz, 2H), 5.53-5.58 (dd, J = 11.6 Hz, 1H), 7.13-7.84(m, 9H); ^{13}C NMR (400 MHz, DMSO-d_6) 27.97, 41.87, 59.42, 125.54-141.58, 155.97, 177.12, 162.57, 162.91, 160.15; UV Spectrum (10ppm) λ_{max} 289.2 nm; Theoretical mass 379.1, LC-MS (m/z, I %), 380.1 [$(M+H)^+$, 100%]; HPLC Purity % Area 97.52 %, RT 5.29 mins.

1-(2-(3-(4-fluorophenyl)-5-phenyl-4,5-dihydro-1H-pyrazol-1-yl)-2-oxoethyl)pyrrolidine-2,5-dione (S8) Yield 0.8g (40 %); M.P. 184.6°C; White crystalline solid; IR (cm^{-1}) 2821, 1699, 1672, 1602, 1151; ^{1}H NMR (400 MHz, DMSO-d_6, δ ppm) 2.70(s, 4H), 3.16-3.22 (dd, J = 18.2 Hz, 1H), 3.87-3.95(m, 1H), 4.54-4.67(q, J = 17.4 Hz, 2H), 5.52-5.57(dd, J = 11.8 Hz, 1H), 7.19-7.91(m, 9H); ^{13}C NMR (400 MHz, DMSO-d_6) 27.97, 42.07, 60.17, 115.57-141.58, 155.06, 177.12, 162.20, 162.84, 164.68; UV Spectrum (10ppm) λ_{max} 289.2 nm; Theoretical mass 379.1, LC-MS (m/z, I %), 380.1 [$(M+H)^+$, 100%]; HPLC Purity % Area 97.76 %, RT 5.27 mins.

1-(2-oxo-2-(3-phenyl-5-(thiophen-2-yl)-4,5-dihydro-1H-pyrazol-1-yl)ethyl)pyrrolidine-2,5-dione (S9) Yield 1.0g (50 %); M.P. 189.9°C; White crystalline solid; IR (cm^{-1}) 2966, 1703, 1676, 1602; ^{1}H NMR (400 MHz, DMSO-d_6, δ ppm) 2.73(s, 4H), 3.37-3.39(m, 1H), 3.87-3.94(m, 1H), 4.49-4.60 (m, 2H), 5.84-5.88(dd, J = 11.2 Hz, 1H), 6.94-6.96(t, J= 4.4 Hz, 1H), 7.03-7.04(d, J= 3.2 Hz, 1H), 7.41-7.42(m, 1H), 7.41-7.51(m, 3H), 7.84-7.86(m, 2H); ^{13}C NMR (400 MHz, DMSO-d_6) 28, 41.62, 55.57, 124.89-143.91, 156.10, 177.11, 162.8; UV Spectrum (10ppm) λ_{max} 289.1 nm; Theoretical mass 367.1, LC-MS (m/z, I %), 368.1 [$(M+H)^+$, 100%]; HPLC Purity- % Area 98.88 %, RT 4.36 mins.

1-(2-(5-(furan-2-yl)-3-phenyl-4,5-dihydro-1H-pyrazol-1-yl)-2-oxoethyl)pyrrolidine-2,5-dione (S10) Yield 0.9g (45 %); M.P. 216.2°C; White crystalline solid; IR (cm^{-1}) 2920, 1703, 1674, 1600, 1168; ^{1}H NMR (400 MHz, DMSO-d_6, δ ppm) 2.73(s, 4H), 3.38-3.41(m, 1H), 3.70-3.82(m, 1H), 4.49-4.59(m, 2H), 5.63-5.69(dd, J = 11.6 Hz, 1H), 6.33(m, 1H), 6.39(m, 1H), 7.50-7.59 (m, 4H), 7.83-8.85(m, 1H); ^{13}C NMR (400 MHz, DMSO-d_6): 27.99, 38.16, 53.64, 107.44-142.59, 151.87, 177.15, 162.84; UV Spectrum (10ppm) λ_{max} 288.1 nm; Theoretical mass 351.1, LC-MS (m/z, I %), 352.1 [$(M+H)^+$, 100%]; HPLC Purity- % Area 98.38 %, RT 3.73 mins.

1-(2-(3-(4-fluorophenyl)-5-(furan-2-yl)-4,5-dihydro-1H-pyrazol-1-yl)-2-oxoethyl)pyrrolidine-2,5-dione (S11) Yield 1.11 g (55.5%); M.P. 175.4°C; White crystalline solid; IR (cm^{-1}) 2966, 1703, 1666, 1602, 1168; ^{1}H NMR (400 MHz, DMSO-d_6, δ ppm) 2.73(s, 4H), 3.44-3.45 (m, 1H), 3.78-3.82 (m, 1H), 4.47-4.57(m, 2H), 5.63-5.67(dd, J = 11.8 Hz, 1H), 6.32(d, J = 2.8, 1H), 6.39(d, J = 1.6, 1H), 7.32-7.36(t, J= 8.8 2H), 7.57(S, 1H), 7.90-8.92 (m, 1H), 7.57(s, 2H); ^{13}C NMR (400 MHz, DMSO-d_6) 27.99, 38.24, 53.75, 107.46-142.59, 151.83, 162.24-162.84, 177.15, 162.84; UV Spectrum (10ppm) λ_{max} 287.5nm; Theoretical mass 369.1, LC-MS (m/z, I %), 370.1 [$(M+H)^+$, 100%]; HPLC Purity- % Area 98.61 %, RT 3.83 mins.

1-(2-(3-(2,4-difluorophenyl)-5-(3,4-dimethoxyphenyl)-4,5-dihydro-1H-pyrazol-1-yl)-2-oxo ethyl)pyrrolidine-2,5-dione (S12) Yield 1.25 g (62.5%); M.P. 116.3 °C; White crystalline solid; IR (cm^{-1}) 2913, 1703, 1674, 1602, 1166; ^{1}H NMR (400 MHz, DMSO-d_6, δ ppm) 2.71(s, 4H), 3.13-3.20 (dd, J=18.4 Hz, 1H), 3.72-3.73 (s, 1H), 3.89-3.97(m, 1H), 4.50-4.54 (d, J= 16.8 Hz, 1H), 4.61-4.65 (d, J= 16.8 Hz, 1H), 5.45-5.49 (dd, J = 11.6 Hz, 1H), 6.70-6.73 (dd, J = 8.4 Hz, 1H), 6.78-6.79 (d, J = 1.8, 1H), 6.88-6.90 (d, J = 8.4, 1H), 7.20-7.25 (m, 1H), 7.37-7.43 (m, 1H), 7.92-8.03 (m, 1H); ^{13}C NMR (400 MHz, DMSO-d_6) 27.95, 44.03, 55.36-55.50, 59.52, 104.82-148.77, 151.51, 148.77, 148.06, 177.13, 163.02; UV Spectrum (10ppm) λ_{max} 286.2 nm; Theoretical mass

457.1, LC-MS (m/z, I %), 458.1 [$(M+H)^+$, 100%]; HPLC Purity- % Area 97.71 %, RT 4.87 mins.

1-(2-(5-(3,4-dichlorophenyl)-3-phenyl-4,5-dihydro-1H-pyrazol-1-yl)-2-oxoethyl)pyrrolidine-2,5-dione (S13) Yield 0.8g (40 %); M.P. 209.1°C; White crystalline solid; IR (cm^{-1}) 2803, 1702, 1676, 1601, 1168, 759; ^{1}H NMR (400 MHz, DMSO-d_6, δ ppm) 2.71(s, 4H), 3.12-3.17 (dd, J=18.2 Hz, 1H), 3.93-4.01 (m, 1H), 4.56-4.72 (d, J= 17.2 Hz, 2H), 5.71-5.76(dd, J= 12 Hz, 1H), 7.14-7.16(d, J = 8.4 Hz, 1H), 7.37-7.39 (m, 1H), 7.48-7.49 (m, 3H), 7.64 (d, J= 1.2 Hz, 2H), 7.80-7.82 (m, 1H); ^{13}C NMR (400 MHz, DMSO-d_6) 27.99, 40.63, 57.51, 126.90-132.80, 131.93, 156.09, 177.10, 163.09; UV Spectrum (10ppm) λ_{max} 287.6 nm; Theoretical mass 429.06, LC-MS (m/z, I %), 430.1 [$(M+H)^+$, 100%]; HPLC Purity- % Area 97.52 %, RT 11.43 mins.

4.3 *In vitro* antiproliferative effects by MTT assay

K562 cells (Chronic myeloid leukemia), MCF7 (Breast cancer) and HT29 (Colon cancer), were obtained from National Center for Cell Sciences (NCCS), Pune. K562 cells were kept as suspension in RPMI 1640 medium (Thermo fisher scientific), supplied with 10% FBS (fetal bovine serum, Gibco, Invitrogen) and 1% anti-microbial antimycotic 100X solution (100 units/mL of penicillin, 100 µg/mL of streptomycin, and 0.25 µg/mL of Gibco Amphotericin B). MCF7 and HT29 cells were maintained under similar conditions except the medium used was DMEM (Thermo fisher scientific). All cells were kept up in a humidified 5% CO_2 air environment at 37˚C.

MTT assay was employed to find out cytotoxic potential of S1-S13 on proliferation of K562, MCF7 and HT29 cells. The assay was conducted as described earlier [41]. Quickly, the cells were seeded at a density of around 5×10^3 cells/well in a flat 96-well plate and kept overnight at 37 ºC in 95% humidity and supplied with 5% CO_2. Increasing concentrations of compounds were made in DMSO and added to the cells. The maximum concentration of DMSO in the individual assay, was <1.5% and demonstrated no cell lethality. The cells were incubated with test compounds for 48 h. then, plates were centrifuged at 300 g at 4°C for 5 minutes and were washed twice with phosphate buffer. 20 µL of the MTT staining reagent (5mg/ml in phosphate buffer) was added to each well and the plates were incubated at 37ºC. After 4 h, 100 µL of dimethyl sulfoxide (DMSO) was added to each well so as to solubilize the formazan crystals, and absorbance was recorded with a 570 nm utilizing micro plate reader.

4.4 Cell Cycle analysis and Bcl-2 expression

Effects of **S2** on cell cycle distribution and apoptosis signalling pathways were studied in K562 cells. The cells were seeded in 96-well plates and incubated at 37 ºC in a 5% CO_2 atmosphere during 18 h, thereafter **S2** was added to the cells, and the incubation was continued for 48 or 72 h more. Final concentrations of **S2** were 47.25 µM, 23.63 µM, 11.81 µM. HBSS was used in control group. More than 2000 cells were analysed in every sample using Muse® Cell Analyser and Muse® Detection Kits (EMD Millipore Corporation) in triplicate. Muse® Cell Cycle Kit (MCH100106 EMD Millipore Corp., USA) and Muse® Bcl-2 Activation Dual Detection Kit (MCH200105 EMD Millipore Corp., USA) were used in accordance with manufacturer's manual. Results are presented as mean ± SD.

4.5 Molecular Docking

Two crystal structures of Bcl-2 (PDB-IDs 4AQ3 and 6GL8) were obtained from RCSB Protein Data Bank and subjected to the Quickprep procedure of MOE 2019 software (Chemical Computing Group ULC, Canada) including correcting problems with the structure and 3D-protonation. Then the native ligands were removed from the receptor proteins, also using MOE. Docking was carried out using Autodock Vina (http://vina.scripps.edu/)[55] embedded in PyRx (https://pyrx.sourceforge.io/)[56], a virtual screening software for computational drug discovery. The prepared protein structures and mol2 files of the ligands were loaded into PyRx and converted to the required pdbqt file format. The original ligands were docked back in their binding site (redocking) to validate the docking setting. Subsequently, two stereo isomers of **S2** were docked into the same receptor proteins. To consider the observed flexibility of binding groove amino acids, docking was followed by an energy minimization step within a radius of 10 Å around the respective ligand using MOE 2019 and AMBER14 force field.

4.6 *In vivo* tumor regression in HT-29 xenografts

Anticancer effect of **S2** was evaluated in HT-29 colorectal adenocarcinoma xenografts in Balb/c nude mice. Male Balb/c nude mice 6–8 weeks of age were obtained from N.N. Blokhin Cancer Research Center. The mice were housed in a pathogen-free environment under controlled conditions of light and humidity and received food and water ad libitum. HT-29 cells (5×10^6) were implanted subcutaneously with Matrigel® (1:1; Matrix) into left flank of mice. Once the mean tumor volume reached ~65 mm^3, animals were randomized into treatment groups (n=6–10), and dosing with **S2** was initiated (day 1): 50 mg/kg i.p. (intraperitoneally) or *per os* (oral route) daily during 20 days (cumulative dose 1 g/kg).Tumor sizes and body weights were measured twice weekly. Tumor volume was calculated by the formula: $V=\pi/6\cdot(L\cdot W\cdot H)$, where L is length, W is width and H is height of tumor. Efficiency assessment was carried out using TGI (tumor growth inhibition). Statistical analyses of *in vivo* research were performed using SPSS V. 22.0 comparing continuous variables by non-parametrical Mann-Whitney U. Data are expressed as mean ± standard deviation (SD).

Ethical statement

All animal studies were performed according to the European Convention for the Protection of Vertebrate Animals used for Experimental and Other Scientific Purposes. All animal protocols were approved by the local ethical committee of N.N. Blokhin Cancer Research Center.

Declaration of Competing Interest.

The authors declare that they have no known competing financial interests.

Acknowledgements

This study was supported by Indo-Poland joint research program grant from Department of Science and Technology (DST) with reference number DST/INT/Pol/P-27/2016 (to CSR). The

biological studies were supported by Russian Scientific Foundation RSF grant 18-75-10008(to VPS).

Keywords

•Pyrrolidine-2,5-dione • Synthesis • Cytotoxicity • Docking • Antitumor • Bcl-2 • Pyrazoline • *in vivo*

References

[1] A. Colombo, C. Cipolla, M. Beggiato, D. Cardinale, *Curr Cardiol Rep* **2013**, *15*, 362.
[2] N. Milman, L. Ginini, Z. Gil, *Drug Resistance Updates* **2019**, *45*, 1.
[3] B.S.P. Sandor Eckhardt, *CMCACA* **2002**, *2*, 419.
[4] A. Ameri, G. Khodarahmi, H. Forootanfar, F. Hassanzadeh, G.-H. Hakimelahi, *Chem. Biodiversity* **2018**, *15*, e1700518.
[5] D. Havrylyuk, B. Zimenkovsky, O. Vasylenko, A. Gzella, R. Lesyk, *J. Med. Chem.* **2012**, *55*, 8630.
[6] A. Saeed, P.A. Mahesar, P.A. Channar, F.A. Larik, Q. Abbas, M. Hassan, H. Raza, S.-Y. Seo, *Chem. Biodiversity* **2017**, *14*, e1700035.
[7] V.R. Solomon, C. Hu, H. Lee, *Bioorganic & Medicinal Chemistry* **2009**, *17*, 7585.
[8] S. Chauhan, S. Paliwal, R. Chauhan, *Synthetic Communications* **2014**, *44*, 1333.
[9] K.M. Kasiotis, E.N. Tzanetou, S.A. Haroutounian, *Front. Chem.* **2014**, *2*.
[10] F.M. Awadallah, G.A. Piazza, B.D. Gary, A.B. Keeton, J.C. Canzoneri, *European Journal of Medicinal Chemistry* **2013**, *70*, 273.
[11] P. Rathore, S. Yaseen, S. Ovais, R. Bashir, R. Yaseen, A.D. Hameed, M. Samim, R. Gupta, F. Hussain, K. Javed, *Bioorganic & Medicinal Chemistry Letters* **2014**, *24*, 1685.
[12] H. Fahmy, N. Khalifa, M. Ismail, H. El-Sahrawy, E. Nossier, *Molecules* **2016**, *21*, 271.
[13] C. Fan, J. Zhao, B. Zhao, S. Zhang, J. Miao, *Chem. Res. Toxicol.* **2009**, *22*, 1517.
[14] R.F. George, M.A. Fouad, I.E.O. Gomaa, *European Journal of Medicinal Chemistry* **2016**, *112*, 48.
[15] G. Nitulescu, C. Draghici, O. Olaru, *IJMS* **2013**, *14*, 21805.
[16] Y.-J. Qin, Y. Li, A.-Q. Jiang, M.-R. Yang, Q.-Z. Zhu, H. Dong, H.-L. Zhu, *Eur J Med Chem* **2015**, *94*, 447.
[17] L.-W. Zheng, Y. Li, D. Ge, B.-X. Zhao, Y.-R. Liu, H.-S. Lv, J. Ding, J.-Y. Miao, *Bioorganic & Medicinal Chemistry Letters* **2010**, *20*, 4766.
[18] E.D. Deeks, *Drugs* **2015**, *75*, 1393.
[19] F.A. Luzzio, D.Y. Duveau, E.R. Lepper, W.D. Figg, *J. Org. Chem.* **2005**, *70*, 10117.
[20] J. Best, C. Schotten, G. Lohmann, G. Gerken, A. Dechêne, *Expert Opinion on Pharmacotherapy* **2017**, *18*, 727.
[21] K.S. Devi, P. Subramani, S. Parthiban, N. Sundaraganesan, *Journal of Molecular Structure* **2020**, *1203*, 127403.
[22] S.H. Han, S. Kim, U. De, N.K. Mishra, J. Park, S. Sharma, J.H. Kwak, S. Han, H.S. Kim, I.S. Kim, *J. Org. Chem.* **2016**, *81*, 12416.
[23] D.V. Kaminskyy, R.B. Lesyk, *Biopolym. Cell* **2010**, *26*, 136.
[24] E.L. Luzina, A.V. Popov, *Journal of Fluorine Chemistry* **2014**, *168*, 121.
[25] N.P. Milosevic, V. Kojic, J. Curcic, D. Jakimov, N. Milic, N. Banjac, G. Uscumlic, R. Kaliszan, *Journal of Pharmaceutical and Biomedical Analysis* **2017**, *137*, 252.
[26] A. Sharma, T. Pathan, R. Mohan, C. S. Ramaa, *LDDD* **2011**, *8*, 843.
[27] H. Joshi, K. Marulkar, V. Gota, C. S. Ramaa, *ACAMC* **2017**, *17*, 524.
[28] T. Pal, H. Joshi, C.S. Ramaa, *ACAMC* **2014**, *14*, 872.
[29] V. Patil, K. Tilekar, S. Mehendale-Munj, R. Mohan, C.S. Ramaa, *European Journal of Medicinal Chemistry* **2010**, *45*, 4539.
[30] A. Kabir, K. Tilekar, N. Upadhyay, C.S. Ramaa, *ACAMC* **2019**, *18*, 1551.
[31] S. Saha, D.S.Z. Chan, C.Y. Lee, W. Wong, L.S. New, W.K. Chui, C.W. Yap, E.C.Y. Chan, H.K. Ho, *European Journal of Pharmacology* **2012**, *697*, 13.
[32] A. Daina, O. Michielin, V. Zoete, *Sci Rep* **2017**, *7*, 42717.
[33] A. Daina, O. Michielin, V. Zoete, *J. Chem. Inf. Model.* **2014**, *54*, 3284.
[34] Md.L. Amin, *Drug Target Insights* **2013**, *7*, DTI.S12519.
[35] C.A. Lipinski, F. Lombardo, B.W. Dominy, P.J. Feeney, *Advanced Drug Delivery Reviews* **2001**, *46*, 3.
[36] I. Muegge, S.L. Heald, D. Brittelli, *J. Med. Chem.* **2001**, *44*, 1841.
[37] D.F. Veber, S.R. Johnson, H.-Y. Cheng, B.R. Smith, K.W. Ward, K.D. Kopple, *J. Med. Chem.* **2002**, *45*, 2615.
[38] W.J. Egan, K.M. Merz,, J.J. Baldwin, *J. Med. Chem.* **2000**, *43*, 3867.
[39] A.K. Ghose, V.N. Viswanadhan, J.J. Wendoloski, *J. Comb. Chem.* **1999**, *1*, 55.
[40] A. Daina, V. Zoete, *ChemMedChem* **2016**, *11*, 1117.
[41] K. Tilekar, N. Upadhyay, N. Jänsch, M. Schweipert, P. Mrowka, F.J. Meyer-Almes, C.S. Ramaa, *Bioorganic Chemistry* **2020**, *95*, 103522.
[42] N. Upadhyay, K. Tilekar, N. Jänsch, M. Schweipert, J.D. Hess, L. Henze Macias, P. Mrowka, R.J. Aguilera, J. Choe, F.-J. Meyer-Almes, C.S. Ramaa, *Bioorganic Chemistry* **2020**, *100*, 103934.
[43] C.A. Tucker, A.I. Kapanen, G. Chikh, B.G. Hoffman, A.H. Kyle, I.M. Wilson, D. Masin, R.D. Gascoyne, M. Bally, R.J. Klasa, *Molecular Cancer Therapeutics* **2008**, *7*, 749.
[44] C.-M. Park, M. Bruncko, J. Adickes, J. Bauch, H. Ding, A. Kunzer, K.C. Marsh, P. Nimmer, A.R. Shoemaker, X. Song, S.K. Tahir, C. Tse, X. Wang, M.D. Wendt, X. Yang, H. Zhang, S.W. Fesik, S.H. Rosenberg, S.W. Elmore, *J. Med. Chem.* **2008**, *51*, 6902.
[45] C. Tse, A.R. Shoemaker, J. Adickes, M.G. Anderson, J. Chen, S. Jin, E.F. Johnson, K.C. Marsh, M.J. Mitten, P. Nimmer, L. Roberts, S.K. Tahir, Y. Xiao, X. Yang, H. Zhang, S. Fesik, S.H. Rosenberg, S.W. Elmore, *Cancer Research* **2008**, *68*, 3421.
[46] M.D. Wendt, *Expert Opinion on Drug Discovery* **2008**, *3*, 1123.
[47] A. Pinelli, C. Godio, A. Laghezza, N. Mitro, G. Fracchiolla, V. Tortorella, A. Lavecchia, E. Novellino, J.-C. Fruchart, B. Staels, M. Crestani, F. Loiodice, *J. Med. Chem.* **2005**, *48*, 5509.
[48] L. Porcelli, F. Gilardi, A. Laghezza, L. Piemontese, N. Mitro, A. Azzariti, F. Altieri, L. Cervoni, G. Fracchiolla, M. Giudici, U. Guerrini, A. Lavecchia, R. Montanari, C. Di Giovanni, A. Paradiso, G. Pochetti, G.M. Simone, P. Tortorella, M. Crestani, F. Loiodice, *J. Med. Chem.* **2012**, *55*, 37.
[49] J. Wen, Q. Niu, J. Liu, Y. Bao, J. Yang, S. Luan, Y. Fan, D. Liu, L. Zhao, *Bioorganic & Medicinal Chemistry Letters* **2016**, *26*, 375.
[50] J. Yang, G. Cheng, Q. Xu, S. Luan, S. Wang, D. Liu, L. Zhao, *Bioorganic & Medicinal Chemistry* **2018**, *26*, 1418.
[51] C. Zagni, A. Citarella, M. Oussama, A. Rescifina, A. Maugeri, M. Navarra, A. Scala, A. Piperno, N. Micale, *IJMS* **2019**, *20*, 945.

[52] K. Chen, Y.-L. Zhang, J. Fan, X. Ma, Y.-J. Qin, H.-L. Zhu, *European Journal of Medicinal Chemistry* **2018**, *156*, 722.
[53] D. Havrylyuk, B. Zimenkovsky, O. Vasylenko, A. Gzella, R. Lesyk, *J. Med. Chem.* **2012**, *55*, 8630.
[54] K.M. Amin, A.A.M. Eissa, S.M. Abou-Seri, F.M. Awadallah, G.S. Hassan, *European Journal of Medicinal Chemistry* **2013**, *60*, 187.
[55] O. Trott, A.J. Olson, *J. Comput. Chem.* **2009**, NA.
[56] S. Dallakyan, A.J. Olson, in *Chemical Biology* (Eds: J.E. Hempel, C.H. Williams, C.C. Hong), Springer New York, New York, NY **2015**, 243.

Entry for the Table of Contents

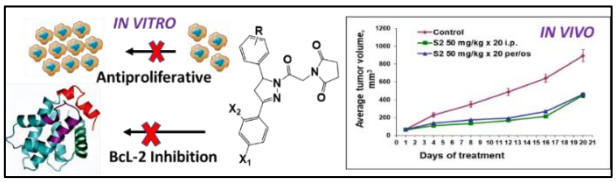

hybrids of Pyrazoline and Pyrrolidine-2,5-dione as antitumor agents with oral bioavailability and tumor regression efficacy

- In vitro antiproliferative effects of compound S2 in HT29, MCF-7 and K562 cell lines were in sub-micromolar range.
- Compound S2 found to cause in vivo tumor regression by intraperitoneal and Oral route in HT29 xenografts.
- Compound S2 exhibited dose dependent inhibition of anti-apoptotic protein, Bcl-2 and corelated well with docking studies.